JCI The Journal of Clinical Investigation

uPAR isoform 2 forms a dimer and induces severe kidney disease in mice

Changli Wei, … , M. Amin Arnaout, Jochen Reiser

J Clin Invest. 2019. https://doi.org/10.1172/JCI124793.

Research In-Press Preview **Nephrology**

Soluble urokinase plasminogen activator receptor (suPAR) is an immune-derived circulating signaling molecule that has been implicated in chronic kidney disease such as focal segmental glomerulosclerosis (FSGS). Typically, native uPAR (isoform 1) translates to a three-domain protein capable of binding and activating integrins, yet the function of additional isoforms generated by alternative splicing is unknown. Here, we characterized mouse uPAR isoform 2 (msuPAR2), encoding domain I and nearly one-half of domain II, as a dimer in solution, as revealed by 3D electron microscopy structural analysis. In vivo, msuPAR2 transgenic mice exhibited signs of severe renal disease characteristic of FSGS with proteinuria, loss of kidney function and glomerulosclerosis. Sequencing of the glomerular RNAs from msuPAR2-Tg mice revealed differentially expressed gene signature that includes upregulation of the suPAR receptor *Itgb3*, encoding β3 integrin. Crossing msuPAR2-transgenic mice with three different integrin β3 deficiency models rescued msuPAR2-mediated kidney function. Further analyses indicated a central role for β3 integrin and c-Src in msuPAR2 signaling and in human FSGS kidney biopsies. Administration of Src inhibitors reduced proteinuria in msuPAR2-transgenic mice. In conclusion, mouse uPAR isoform 2 may play an important role in certain forms of scarring kidney disease.

uPAR isoform 2 forms a dimer and induces severe kidney disease in mice

Changli Wei[1], Jing Li[1], Brian D. Adair[2], Ke Zhu[1], Jian Cai[3], Michael Merchant[3], Beata Samelko[1], Zhongji Liao[4], Kwi Hye Koh[1], Nicholas J Tardi[1], Ranadheer R. Dande[1], Shuangxin Liu[1], Jianchao Ma[1], Salvatore Dibartolo[1], Stefan Hägele[1], Vasil Peev[1], Salim S Hayek[5], David J Cimbaluk[6], Melissa Tracy[1], Jon Klein[3], Sanja Sever[2], Sanford J Shattil[4], M. Amin Arnaout[2], Jochen Reiser[1]

[1]Department of Medicine, Rush University Medical Center, Chicago, IL
[2]Harvard Medical School, Division of Nephrology, Massachusetts General Hospital, Charlestown, MA
[3]University of Louisville, Louisville, KY
[4]Department of Medicine, University of California-San Diego, La Jolla, CA
[5]University of Michigan Frankel Cardiovascular Center, Ann Arbor, MI
[6]Department of Pathology, Rush University Medical Center, Chicago, IL

Corresponding should be addressed to:

Dr. Changli Wei MD, PhD
Department of Medicine
Rush University Medical Center
1735 W Harrison ST
Cohn Research Bldg, 7th Floor, Suite 716
Chicago, IL, 60612
Changli_Wei@rush.edu

Jochen Reiser MD, PhD
Department of Medicine
Rush University Medical Center
1715 W Congress Parkway
Kellogg Bldg, Suite 1003,
Chicago, IL 60612
Jochen_Reiser@rush.edu

Conflict of Interest Statement
JR and SS are inventors on pending and issued patents related to antiproteinuric therapies. They stand to gain royalties from present and future commercialization. They also are cofounders and advisors to TRISAQ, a biotechnology company. CW has a pending patent on suPAR in diabetes. He stands to gain royalties from future commercialization products concerning this application.

Abstract

Soluble urokinase plasminogen activator receptor (suPAR) is an immune-derived circulating signaling molecule that has been implicated in chronic kidney disease such as focal segmental glomerulosclerosis (FSGS). Typically, native uPAR (isoform 1) translates to a three-domain protein capable of binding and activating integrins, yet the function of additional isoforms generated by alternative splicing is unknown. Here, we characterized mouse uPAR isoform 2 (msuPAR2), encoding domain I and nearly one-half of domain II, as a dimer in solution, as revealed by 3D electron microscopy structural analysis. In vivo, msuPAR2 transgenic mice exhibited signs of severe renal disease characteristic of FSGS with proteinuria, loss of kidney function and glomerulosclerosis. Sequencing of the glomerular RNAs from msuPAR2-Tg mice revealed differentially expressed gene signature that includes upregulation of the suPAR receptor *Itgb3*, encoding β3 integrin. Crossing msuPAR2-transgenic mice with three different integrin β3 deficiency models rescued msuPAR2-mediated kidney function. Further analyses indicated a central role for β3 integrin and c-Src in msuPAR2 signaling and in human FSGS kidney biopsies. Administration of Src inhibitors reduced proteinuria in msuPAR2-transgenic mice. In conclusion, mouse uPAR isoform 2 may play an important role in certain forms of scarring kidney disease.

Introduction

Urokinase receptor or urokinase plasminogen activator receptor (uPAR) is a GPI–anchored protein that acts as a receptor for pro-urokinase and facilitates the generation of activated plasmin. Removal of the GPI-anchor from uPAR by phosphatidylinositol-specific phospholipase C generates soluble uPAR (suPAR) (1), which can be detected in different body fluids such as blood and urine (2). A large body of evidence has shown that suPAR could serve both as an inflammatory biomarker and as a signaling molecule (2). A role for suPAR in kidney disease was first noted in patients with focal segmental glomerulosclerosis (FSGS), in whom high levels were associated with recurrence of FSGS post-transplantation (3). Elevated suPAR accounting for kidney injury is thought to originate from bone marrow myeloid stem cells (4). We have suggested that suPAR promotes pathologic changes in kidney function mainly through activation of αvβ3 integrin on podocytes (3). This activation is enhanced in the presence of CD40 autoantibodies or ApoL1 risk variants (5,6). High suPAR levels have been associated with a long-term decline in renal function and incident CKD in a variety of patient cohorts (cardiovascular, healthy middle-aged, pre-diabetic, dialysis patients) (7-10), suggesting a role for suPAR as a biomarker and potential risk factor for kidney disease. The underlying reasons for the difference in clinical presentation in suPAR-associated FSGS and non-FSGS kidney disease are unclear, and may be due to different isoforms of suPAR.

Notably, uPAR has multiple isoforms in human and mice due to alternative splicing of the seven encoding exons in both species (11,12). Their distinct

biological roles however are not yet clear. As part of our initial study in defining the role of suPAR in kidney disease, we cloned mouse uPAR isoform 2 (msuPAR2) from cultured mouse podocytes and showed its transduced expression caused rapid nephropathy in mice (3). In contrast, transgenic mouse models expressing soluble form of mouse uPAR isoform 1 (msuPAR1) did not develop any renal phenotype over a 6-week period (13), but rather required several months (4). Similarly, administration of recombinant msuPAR1 per se did not cause proteinuria in mice (14), suggesting that msuPAR1 and msuPAR2 might have diverse roles with regard to kidney pathogenesis. In this study, we purified msuPAR2 protein from HEK cells and characterized its structure as a dimer. In vivo, utilizing different transgenic mouse models, we found msuPAR2, but not msuPAR1 induces a severe kidney disease characteristic of FSGS via the $\alpha v\beta 3$-Src signaling axis.

Results

msuPAR2 forms a dimer in solution

msuPAR1 and msuPAR2 share 100% homology for uPAR domain I (D1) and the N-terminal portion of domain II (D2), while msuPAR2 lacks the C-terminal end of D2, and D3 domain, and thus GPI anchor (**Supplemental Figure 1**). To characterize the corresponding proteins, we cloned and expressed msuPAR1 (without the GPI anchor) and msuPAR2 in HEK 293 cells. Both, msuPAR1 and msuPAR2 proteins are glycosylated (**Figure 1A**). Under reducing conditions, msuPAR1 migrated as a single band between 50-60 kDa before and ~35 kDa after treatment with PNGaseF, while msuPAR2 migrated at 32-33 kDa before and ~25 kDa after deglycosylation (**Figure 1A, Supplemental Figure 2A**). msuPAR1 and msuPAR2 were verified by mass spectrometry analysis after deglycosylation (**Figure 1B**). Under non-reducing conditions, msuPAR1 migrated as multiple bands consistent with a monomer, a dimer and higher-order multimers. By contrast, msuPAR2 remained as monomer (**Supplemental Figure 2B**). Under native conditions, while msuPAR1 migrated as multiple bands, msuPAR2 presented as one band at ~ 66 kDa, suggesting formation of homo-dimers (**Supplemental Figure 2C**). As the structure of msuPAR1 was already solved by X-ray crystallography (15), we examined msuPAR2 by electron microscopy (EM). Reference-free class averages of msuPAR2 particles displayed clear multi-domain features (**Supplemental Figure 3**) with three to four distinct domains with diameters of ~70-100 Å. The expressed construct possesses a full D1 domain and a small, disulfide-linked region from D2 (**Figure**

1C). These known folding domains would not have a diameter greater than 50 Å, indicating that the particles visualized in the micrographs are too large to be monomers. Single particle reconstructions with an imposed two-fold symmetry provided a good fit for the reference-free particle data and converged with a final resolution of 17 Å (**Supplementary Figure 3**). The resulting map indicates an isosurface set to enclose density for the expected volume of the 25 kDa msuPAR2 core protein. At this isosurface, two symmetry-related domains provide a good fit for the intact D1 domain (**Figure 1C**). These domains are not interacting with one another but are connected by a third domain containing the dimer interface, and are of suitable size to contain the N-terminal portion of D2 in the construct, but the resolution does not permit precise fitting of this domain into the map. Taken together, our data imply that in contrast to msuPAR1, msuPAR2 forms a dimer with distinct structural characteristics.

msuPAR2 is detected in adipocytes, blood and urine

Since msuPAR2 has distinct protein features from msuPAR1, we next generated msuPAR2 transgenic mouse model to examine its functional relevance. The transgene was built under the control of an AP2 promoter with a secretion signal peptide and a C-terminal Myc tag (**Figure 2A**). msuPAR2 expressing mice were fertile, viable, and born at a normal Mendelian ratio. In parallel, we examined msuPAR1 transgenic mice that were generated exactly the same way for comparison. We have shown using an ELISA assay that msuPAR1-Tg mice had a high level of msuPAR1 in both serum and urine

samples (4). Since there is no ELISA kit available for a specific msuPAR2 measurement, we firstly examined adipose tissues for msuPAR2 expression driven by AP2 promoter. Compared to littermate controls, msuPAR2 mRNA expression increased by 11-fold in msuPAR2-Tg mice (**Figure 2B**). The msuPAR2 expression in adipocytes at the protein level was confirmed by immunohistochemical staining with an anti-c-Myc antibody (**Figure 2C**). Next, we developed a peptide based rabbit polyclonal antibody specific to msuPAR2 (**Supplemental Figure 4A, 4B**). Using this antibody, we performed Western blot analysis with albumin-depleted serum samples. We detected msuPAR2 in the sera of msuPAR2-Tg mice but not in uPAR knockout (KO, *Plaur*$^{-/-}$) or msuPAR1-Tg mice (**Figure 2D**). The specificity of msuPAR2 detection was indicated by msuPAR2 peptide blocking (**Supplemental Figure 4C**). In addition, a msuPAR2 fragment of 10-15 kDa, but not intact msuPAR2, was detected in the urine of msuPAR2-Tg mice (**Figure 2E**). As expected, this msuPAR2 fragment was absent from the urine of msuPAR1-Tg and uPAR KO mice (**Figure 2E**). Moreover, this msuPAR2 fragment was only recognized by the above-described rabbit anti-suPAR2 antibody but not anti-c-Myc antibody. Note that both msuPAR1 and msuPAR2 have C-terminal c-Myc tag in their transgenes, and the anti-c-Myc antibody detected msuPAR1 in the urine of msuPAR1-Tg mice (**Supplemental Figure 5**). Next, we isolated the msuPAR2 fragment from msuPAR2-Tg mice urine and performed LC-MS analysis, which confirmed its identity by detecting the N-terminal but not C-terminal peptides (**Figure 2F).**

msuPAR2-Tg mice develop chronic kidney disease characteristic of FSGS

Circulating suPAR levels have been shown to predict chronic kidney disease progression in humans (7). In msuPAR1-Tg mice, there was no proteinuria at baseline, but one third of animals developed proteinuria after two months of high fat diet (HFD) treatment to stimulate msuPAR1 production via the AP2 promoter (4). Additional analyses revealed that proteinuria in msuPAR1-Tg mice peaked after 6 months of HFD treatment (**Figure 3A**). In contrast, msuPAR2-Tg mice maintained on regular chow developed spontaneous proteinuria starting at 2 months of age (baseline) without HFD treatment, which increased significantly to a severe level by 12 months (**Figure 3B**). Of note, proteinuria was not observed in wild type littermate control mice. Next, we treated msuPAR2-Tg mice with HFD as with msuPAR1-Tg to stimulate the AP2 promoter and thus suPAR production starting from 2 months of age. With HFD treatment, msuPAR2-Tg but not littermate control mice developed accelerated and progressive proteinuria up to 8 months old (**Figure 3C**), at which time death occurred spontaneously in some msuPAR2-Tg mice and thus experimental endpoint was reached. On average of all examined mice, msuPAR2-Tg mice had significantly more proteinuria after 6 months of HFD treatment (albumin/creatinine ratio, ACR, 596.6 ±191.5 mg/g), when compared to msuPAR1-Tg (ACR,165.6 ± 43.7 mg/g, $p<0.05$). As decreased serum albumin level is a key feature of nephrotic syndrome in humans, we measured serum albumin in both msuPAR1-Tg and msuPAR2-Tg mice after 6 months into HFD. We found that msuPAR2-Tg mice had significantly lower serum albumin levels

when compared to littermate controls (30.63 ± 2.50 g/L for msuPAR2-Tg versus 45.84 ± 2.38 g/L for controls, $p<0.0001$) (**Figure 3D**). In contrast, serum albumin levels did not decrease significantly (36.23 ± 5.55 g/L for msuPAR1-Tg versus controls, $p=0.10$).

As a following step, we examined serum markers of kidney function of msuPAR1-Tg and msuPAR2-Tg mice. As shown in **Figure 3E**, serum creatinine was significantly increased in msuPAR2-Tg mice after 6 months into HFD (2.20 ± 0.29 mg/dL for msuPAR2-Tg vs 1.38 ± 0.09 mg/dL for controls, $p<0.05$). In contrast, serum creatinine did not change in msuPAR1-Tg mice (1.34 ± 0.18 mg/dL for msuPAR1-Tg versus controls, $p=0.99$). Similarly, serum BUN levels were significantly increased in msuPAR2-Tg mice (79.06 ± 15.35 mg/dL for msuPAR2-Tg vs 28.74 ± 2.28 mg/dL for littermate controls, $p<0.05$), but not in msuPAR1-Tg (48.20 ± 4.15 mg/dL for msuPAR1-Tg versus controls, $p=0.61$), after 6 months' HFD treatment (**Figure 3F**). Thus, kidney function is significantly impaired in msuPAR2-Tg mice after 6 months of HFD, when elevation of msuPAR2 is shown in the blood circulation.

To explore the kidney histopathology, we performed PAS and H&E staining. Without HFD treatment, msuPAR2-Tg mice were sacrificed at 12 months of age when a high amount of proteinuria was detected. While wild type control mice presented normal kidney morphology, msuPAR2-Tg mice maintained on regular chow showed FSGS-like glomerular features (**Figure 4A, Supplemental Figure 6A**). After 6 months of HFD treatment, 22 ± 3 % of msuPAR2-Tg mice developed kidney pathology that mimicked human FSGS:

some, but not all glomeruli were sclerotic; some segments but not the whole glomerulus were equally affected (**Figure 4B**, **Supplemental Figure 6B**). In contrast, littermate wild type control mice showed only mild glomerular hypertrophy, hypercellularity and hyalinosis but no FSGS-like changes (**Supplemental Figure 6C**). As both wild type control mice and msuPAR1-Tg also received HFD for 6 months, these data suggest that msuPAR2 overexpression but not HFD was associated with FSGS-like kidney disease. Transmission electron microscope (TEM) analysis of msuPAR2-Tg mice revealed that podocyte foot process effacement increased significantly as compared to littermate controls (**Figure 4C, 4D**). Along with progressive proteinuria and impaired kidney function, these results indicate that msuPAR2-Tg mice developed FSGS type changes.

Since we observed glomerular pathology in msuPAR2-Tg mice, we examined if msuPAR2 could be localized in the glomeruli using immunofluorescence labeling. While only minimal levels could be detected in the glomeruli of littermate wild type control mice, msuPAR2 expression was readily observed in the glomeruli of msuPAR2-Tg mice. Of note, msuPAR2 staining did not overlap either with overlapped with with alpha smooth muscle actin (SMA), a marker for mesangial cells (16); nor with VE-cadherin (**Supplemental Fig 7**), a endothelial cell marker (17), but overlapped with the podocyte marker, synaptopodin, indicating that msuPAR2 was localized largely to podocytes (**Figure 4E**). In parallel, we examined the expression of msuPAR1 in the glomeruli of msuPAR1-Tg and msuPAR2-Tg mice. Compared to littermate wild

type control, there was an increase of msuPAR1 in the glomeruli of msuPAR1-Tg mice, partially localized in podocytes. In contrast, no obvious change of msuPAR1 was appreciated in the glomeruli of msuPAR2-Tg mice (**Figure 4F**). Together, these data suggest that circulating msuPAR can be deposited into podocytes.

msuPAR2 induced renal pathogenesis requires β3 integrin

To explore the molecular mechanisms underlying the msuPAR2 induced kidney disease, we performed RNA sequencing on isolated glomeruli from msuPAR2-Tg mice and littermate controls. We found 81 mRNAs including *Itgb3* (encoding β3 integrin) were significantly up-regulated, while 17 mRNAs were down-regulated in suPAR2-Tg glomeruli (**Figure 5A**). When gene enrichment analysis was used to identify key pathways driving these transcriptional changes, the top differentially-expressed pathways in suPAR2-Tg glomeruli included immune response, wound healing, chemotaxis, cell migration, cell proliferation and integrin-mediated pathways (**Figure 5B**).

As β3 integrin has been implicated in our previous studies as a suPAR downstream effector, we chose to corroborate its role in msuPAR2-Tg mice. We first showed that msuPAR2 is a stronger activator of β3 integrin than msuPAR1 in human podocytes (**Figure 5C,D**). Next, we crossed msuPAR2-Tg mice with integrin β3 KO (*Itgb3*$^{-/-}$) mice as well as with two integrin knock-in mouse models, β3ΔRGT and β3EGK respectively (18,19). As indicated in **Figure 6A**, β3ΔRGT knock-in mice lack the 3 C-terminal β3 tail residues- RGT- and exhibit defective

β3 interaction with c-Src and Kindlin-3 (19); whereas RGT is replaced by the corresponding residues of β1, EGK, in β3EGK mice, which rescues β3 interaction with kindlins but not with c-Src (19). As with msuPAR2-Tg mice, msuPAR2-Tg/β3 KO, msuPAR2-Tg/β3ΔRGT and msuPAR2-Tg/β3EGK were then treated with HFD starting at 2 months of age. While msuPAR2-Tg mice developed proteinuria, all three double transgenic mice with impaired β3 integrin expression or function were protected from msuPAR2-induced proteinuria (**Figure 6B**). Finally, kidney histological analysis by PAS staining revealed normal kidneys absent changes characteristic of FSGS in either msuPAR2-Tg/β3 KO, or msuPAR2-Tg/β3ΔRGT or in msuPAR2-Tg/β3EGK mice (**Figure 6C**). These data suggest that msuPAR2 signals through intact integrin β3, and by implication an intact αvβ3 integrin heterodimer is required via c-Src-dependent signaling for msuPAR2-induced kidney injury.

Blocking Src activity reduces proteinuria

To further examine the role of c-Src kinase in msuPAR2-Tg mice, we examined the glomerular c-Src phosphorylation by immunofluorescence. Compared to littermate controls, Src phosphorylation was increased in glomeruli of msuPAR2-Tg mice (**Figure 7A**). Interestingly, the enhancement of c-Src activity was abolished not only in msuPAR2-Tg/β3 KO, but also in msuPAR2-Tg/β3ΔRGT and in msuPAR2-Tg/β3EGK mice. Additionally, the phosphorylation of c-Src was not observed in the glomeruli of msuPAR1-Tg mice (**Figure 7A**).

Taken together, these results indicate that msuPAR2 but not msuPAR1 activate glomerular Src kinase via β3 integrin in the development of kidney disease.

Next, we tested pharmacologic modulation of Src kinase and its effects on proteinuria in msuPAR2-Tg mice. Src inhibitor 1 is a potent, selective, dual site Src tyrosine kinase inhibitor, and it has been used together with PP1 to inhibit Src kinase (20). Thus, we administered both Src inhibitors into msuPAR2-Tg mice via i.p. injection and monitored proteinuria before and after Src inhibitor treatment. While vehicle only administration did not change proteinuria levels, Src inhibitor treatment significantly reduced proteinuria in msuPAR2-Tg mice (**Figure 7B**). Collectively, our data suggest that msuPAR2 induced kidney injuries are mediated by glomerular Src activity, employing the $\alpha v\beta 3$ integrin signaling pathway.

To investigate the implication of c-Src activity in human glomerular kidney disease, we performed immunofluorescent staining for phosphor (p)-c-Src on kidney biopsies from primary FSGS, lupus nephritis (LN), membranoproliferative glomerulonephritis (MPGN) and minimal change disease (MCD). While minimal p-c-Src expression was observed in normal glomeruli, signal intensity was increased in the glomeruli of 6 out of ten examined FSGS patients, but not in any glomeruli from LN, MPGN or MCD patients (**Figure 8**). Overlapping with the podocyte marker synaptopodin indicates that the increase of c-Src activity is largely localized in podocytes. Of note, in these FSGS patients with elevated expression of glomerular p-c-Src, 46%, but not all observed glomeruli were stained positive with variable intensity. In summary, increased glomerular c-Src

phosphorylation is observed in human FSGS kidney as well as in msuPAR2 transgenic mice, blocking c-Src could decrease proteinuria implicating c-Src activation in FSGS.

Finally we investigated if there are alternative human uPAR isoforms expressed in human cells. Quantitative PCR with primer pairs specific for each isoform in peripheral blood mononuclear cells (PBMCs) harvested from healthy human subjects identified mRNA expression of human uPAR isoforms 1 to 4 (H1 to H4) (**Supplemental Figure 8**), indicating that alternative human uPAR isoforms are indeed expressed in humans.

Discussion

Nearly three decades ago, two alternatively spliced mouse uPAR mRNAs were identified in the gastrointestinal tract, with muPAR1 localized in the luminal epithelial cells and muPAR2 found in the basal epithelial cells (11). While most subsequent studies focused on muPAR1, the so-called canonical form, muPAR2 expression at protein level was not confirmed. The present study shows that in contrast to muPAR1, msuPAR2 forms a stable protein and its overexpression induces severe kidney disease in mice, which is dependent on expression of integrin β3, and by extrapolation on outside-in signaling through integrin αvβ3-Src axis.

In contrast to muPAR1, which has 3 intact domains (D1 to D3) and 7 predicted sites of glycosylation, muPAR2 has only intact D1 (encoded by exons 2 and 3), and part of D2 (encoded by exon 4), lacking the remaining of the native protein (part of D2 and all of D3, encoded by exons 5-7), and consequently misses 5 N-glycosylation sites and the GPI anchor. Deduced from its protein sequence, msuPAR2 was assumed to be soluble but unstable due to its number of cysteine residues (21). We originally cloned muPAR2 mRNA from cultured mouse podocytes, performed a HEK cell based co-immunoprecipitation assay with integrin β3, and delivered the muPAR2 transcript into C57BL/6 mice via electroporation as well to develop a kidney disease (3). In this study, we purified msuPAR2 protein from HEK cells and characterized it as a stable protein, forming a dimer comprising D1 and part of D2. The single long strand of β-sheet in the D2 region might pair with the strand from its dimer partner. Note that the

splice junction in msuPAR2 transcript disrupts a disulfide bond between residues 116 and 145, leaving a free cysteine in D2.

Continuing our investigations into animal models, we showed that msuPAR2-Tg mice on regular chow develop spontaneous proteinuric injury from 2 months old, and by 12 months old, glomerular changes that suggest FSGS could be appreciated. With HFD treatment to stimulate AP2 promoter, kidney damages were accelerated as msuPAR2-Tg mice develop hypoalbuminemia and glomerular sclerosis along with reduced renal functions by 8 months old (i.e 6 months after HFD initiation). These data suggest that msuPAR2-Tg mice develop a pathology that resembles human FSGS. By contrast, mice expressing msuPAR1 exhibited kidney glomerular changes with less penetrance with HFD treatment (4). Of note, our msuPAR1-Tg mouse model is different from another msuPAR1 transgenic model reported by Spinale *et al* in which no renal phenotype was observed over 6 weeks (13). The phenotype discrepancy between these two msuPAR1-Tg mouse models likely results from: 1) variances of protein expression site (liver versus fat); 2) the amount of circulating msuPAR1 protein; and 3) differences in exposure of suPAR and HFD to the kidney, and monitoring time.

We previously showed that suPAR isoform 1 interacts with and activate β3 integrin, thereby contributing to the development of FSGS (3). The critical role of integrin β3 was verified here with msuPAR2-induced FSGS in msuPAR2-Tg mice, as lack of integrin β3 protected the msuPAR2-Tg/β3 KO mice from developing proteinuria. More importantly, crossing msuPAR2-Tg mice with two

integrin β3 knock-in models that either lack β3 RGT at the C-terminus of the β3 cytoplasmic tail or where RGT is replaced with EGK from the β1 tail suggests that αvβ3 integrin signaling via Src is necessary for induction of renal pathology. This concept is confirmed by an increased glomerular Src phosphorylation in msuPAR2-Tg mice. Src family kinases belong to non-receptor protein tyrosine kinases and have been implicated in many chronic kidney disease models (22). In particular, Src activity is increased in the animal models of Autosomal dominant polycystic kidney disease (ADPKD) (23). In human patients with ADPKD, bosutinib (SKI-606), an oral dual Src/Bcr-Abl tyrosine kinase inhibitor, could reduce kidney growth compared to placebo (24). Here, we found for the first time that c-Src activation as indicated by c-Src phosphorylation was increased in the podocytes of human FSGS, but not in other examined nephropathies including LN, MPGN and MCD. Additionally, treatment with Src inhibitors, PP1 and Src inhibitor-1 could reduce proteinuria in msuPAR2-Tg mice, not only verifying the involvement of glomerular c-Src kinase activity in FSGS, but also generating a possible novel therapeutic concept via modulating glomerular Src activity.

In humans, we have detected transcripts for each of the four human isoforms in PBMCs from health subjects (Supplemental Figure 8A). Since msuPAR2 is associated with FSGS-like kidney changes in our mouse model, we raise the possibility that overexpression of one or more of these human isoforms may be associated with induction of FSGS in humans. Of these, human isoform 3 appears to be the closest structurally to msuPAR2: It has a deletion of exon 5,

hence lacks the three C-terminal β-strands in domain II. An important difference is that splicing out exon 5 is in-frame, resulting in intact domain III and the GPI anchor, in contrast with the out of frame splice in mouse so that these sequences are absent. Nevertheless, human isoform 3 would most likely form the same dimer assembly as we observe in the msuPAR2 structure. Human isoform 1 is equivalent to canonical mouse uPAR 1, with three intact Ly6/uPAR domains and a GPI anchor sequence. For the remaining two variants, it is difficult to speculate on the impact of exon deletion on structure. Human isoform 4 has an in-frame deletion of exon 6, which contributes the N-terminal sheet assembly to domain III but retains the 3 C-terminal strands of domain III and the GPI anchor. Human isoform 2 shares with msuPAR2 an out-of-frame splice junction following deletion of exon 7; It resembles msuPAR2 in lacking a GPI anchor sequence and a single unpaired β-strand. The C-terminus of this form contains the N-terminal strands from domain III followed by a short, 30 residue sequence generated from mistranslation. As this sequence contains 3 cysteine residues, the effect on structure cannot be predicted. Clearly, further studies on alternative human uPAR isoforms are required to determine their respective roles in the pathogenesis in kidney disease, and to characterize their distinct structures via EM or x-ray crystallography.

In conclusion, we report that overexpression of msuPAR2 forms a dimer in solution. Overexpression of msuPAR2, but not msuPAR1, in mice is associated with a high penetrance FSGS-like morphology in kidneys and laboratory abnormalities that are reminiscent of severe chronic kidney disease.

Mechanistically, msuPAR2 requires the presence of β3 integrin-Src signaling to generate proteinuria. Modulating glomerular Src activity may provide a framework for therapeutic strategies in proteinuria management.

Methods

Cloning, expression and purification

cDNA fragments encoding mouse isoform 1 (Genbank accession NM_011111) and isoform 2 (Genbank accession BC010309) were amplified by PCR with total RNA isolated from cultured mouse podocytes (3,25). msuPAR1 (isoform 1 mature protein, aa 24-297) was subcloned into pSecTag2 vector with c-terminal Myc/His tag (ThermoFisher Scientific), while isoform 2 was subcloned into pSecTag2, p3xFLAG-CMV-14 (E7908, Sigma) or pCMV6-Entry with c-terminal Myc/FLAG tag (Origene) respectively for maximum protein yield. For protein expression and purification, pSecTag2 derived plasmid DNA was transfected and expressed into FreeStyle 293 expression system (ThermoFisher Scientific) for 4-5 days. The cultured medium was then harvested for msuPAR1 or msuPAR2 purification with Pierce Anti-c-Myc agarose gel (ThermoFisher Scientific) following the manufacturer's suggestion. For p3xFLAG-CMV-14 or pCMV6 based msuPAR2 expression and purification, the plasmid DNA was transfected into HEK293T cells and incubated for 48-72 hours. The cells were then harvested, lysed with CelLytic M (Sigma), with the cell lysates centrifuged at 12000 rpm for 20 min. After centrifugation, the supernatants were incubated with Anti-FLAG M2 affinity agarose gel (Sigma) for 2 hours at 4°C. After sufficient washing, msuPAR2 protein was eluted from the anti-FLAG M2 affinity agarose gel with 0.1 M glycine-HCl.

Reducing, non-reducing, and native PAGE

To characterize the above purified mouse suPAR recombinant proteins, 1-2 μg of msuPAR1 or msuPAR2 was incubated with reducing sample buffer containing both LDS and DTT (ThermoFisher Scientific) and heated to 70 degree for 10 min before loaded into NuPAGE gel 4-12% Bis-Tris gel (ThermoFisher Scientific) for electrophoresis. For non-reducing PAGE, equal amounts of msuPAR recombinant proteins was incubated with LDS sample buffer before loaded into NuPAGE gel 4-12% Bis-Tris gel for separation following the manufacturer's instructions. To visualize the proteins, the gels were stained with Gelcode blue reagent (ThermoFisher Scientific). To perform native PAGE, both msuPAR1 and msuPAR2 were buffer exchanged to PBS, and 2-3 μg of each protein was mixed with NativePAGE sample buffer and loaded directly into 4-16% Bis-Tris NativePAGE gel (ThermoFisher Scientific) for electrophoresis at 4 degree for 2 hours. Afterwards, the gel was stained with NOVEX colloidal blue staining kit (ThermoFisher Scientific) to visualize the proteins. Similarly, human uPAR proteins including isoform 1 (R&D Systems), isoform 2 (Origene, corresponding to NM_001005376), isoform 3 (purified in house as above stated) were analyzed with SDS gel under reducing and non-reducing conditions as well, and visualized with Imperial Protein Stain (ThermoFisher Scientific).

Liquid chromatography-mass spectrometry (LC-MS)

Protein samples were deglycosylated with Rapid PNGase (New England BioLabs) according to the manufacturer's protocol and were separated by electrophoresis with a Novex 16% tricine gel. The target bands were washed with

50 mM NH4HCO3 (pH 8.5), reduced with 4 mM DTT, and alkylated with 10 mM iodoacetamide. The samples were then digested with trypsin at 37 degree overnight. Peptides from the samples were extracted with 0.1% formic acid (FA) and acetonitrile (ACN), dried by speed vacuum, dissolved in 1% FA before analyzed by LC-MS.

The trypsinized peptides were analyzed by an UltiMate 3000 nanoLC and Q Exactive HF orbitrap MS system (Thermo Scientific). Peptides in samples were trapped on a μ-precolumn and then transfer to and separated on an in-house packed C18 analytic column (particle size 3.6 μm, 100 μm i.d.×135 mm) with a solvent gradient. The mobile phase consisted of 0.1% FA as Solvent A and ACN with 0.1% FA as Solvent B. The gradient started from 2.5% Solvent B at 200 nL/min, increased from 2.5% to 30% Solvent B from 5 to 20 min, increased from 30% Solvent B at 200 nL/min to 95% Solvent B at 300 nL/min in 5 min, maintained at 95% Solvent B and 300 nL/min for 2.5 min, decreased to 2.5% Solvent B at 300 nL/min in 2.5 min, and maintained at 2.5% Solvent B and 300 nL/min for 10 min. Elute from the column was directly ionized by a nanospray source and analyzed by mass spectrometer in data dependent acquisition (DDA) or parallel reaction monitoring (PRM) mode, that monitors 10 peptides of msuPAR1 and msuPAR2. The mass resolution was 60,000 and 15,000 for MS and MS/MS respectively. AGC, isolation window, and off set were set to 2e5, 2 m/Z, and 0.5 m/Z.

Electron Microscopy analysis of protein

Aliquots of purified msuPAR2 were allowed to adhere for 30 sec – 1 min to carbon-coated copper grids and then stained with 0.75% uranyl formate (Ted Pella, Redding, CA). Images were recorded under minimum electron dose conditions using a CM10 electron microscope (Philips Electron Optics, Hillsboro, OR). Images were recorded at 100 kV on either a Gatan Orius 2k x 2k CCD camera at a nominal magnification of 27,500X generating an image at 2.06 Å/pixel or on Kodak 4489 film at a nominal magnification of 52,000. The film micrographs were digitized with a CoolScan 9000 scanner (Nikon Instruments, Melville, NY) at 8 bits per pixel and 6.35 μm per pixel, subsequently averaged to 12.7 μm per pixel for a final 2.44 Å/pixel. The optical density for each negative was adjusted to give a mean value of ~127 over the total range of 0 to 255.

Image Reconstruction. Image processing was performed with the EMAN2 suite (26). Images were manually evaluated for minimal drift and astigmatism and CTF parameters determined for each micrograph. For preliminary sample evaluation, data from the Gatan Orius CCD was employed. A total of 1334 particles were selected from 31 micrographs and CTF phase corrections applied. Particles were subjected to iterative reference-free classification and averaging and 17 resulting classes used to generate a preliminary 3D model generated without any imposed symmetry using the EMAN2 routine e2initialmodel.py. A starting model displaying C2 symmetry was selected and further refined against the individual particles in the preliminary data set using a multireference alignment algorithm this time with C2 symmetry imposed. The full structural analysis employed data collected on

film. 14,125 particles were selected from 20 micrographs using the semi-automated boxing routine in EMAN2. CTF-corrected particles were subjected to four rounds of iterative reference-free classification and averaging with particles contributing to clearly aggregated averages excluded at each step with particles possessing low signal to noise excluded at the final found, resulting in a final data set of 8455 particles. The data set was split and subjected to iterative refinement in EMAN with the same starting model generated above and imposed C2 symmetry. Progress of the refinement was evaluated by Fourier shell correlation between succeeding models and ceased after the sixth round when subsequent models generated by the refinement failed to display improvement in resolution. Resolution of the final model was determined by a Fourier shell correlation between each independently refined model. The isosurface for the final model was determined from the molecular weight of the full dimer (50 kD), which encloses a volume of 61,000 $Å^3$ using a protein partial specific volume of 0.74 cm^3/g. *Chimera* molecular visualization system was used for visual analysis of the 3D structures and to fit the atomic coordinates for the mouse domain I within the EM density (27). The coordinates for the partial domain II were placed manually.

Mice

C57BL/6j mice (Stock No: 000664), uPAR KO mice (Stock No: 002829), integrin β3 KO mice (Stock No: 004669) were purchased from Jackson Labs. β3ΔRGT and β3EGK mouse models were generated in Dr. Shattil's lab at UCSD.

Generation of msuPAR transgenic mouse models

We generated mouse models that expresses mouse uPAR isoform 1 and isoform 2 respectively. Isoform 1 (msuPAR1-Tg) corresponds to NM_011111 in Genbank, covering the mature protein without GPI anchor. Isoform 2 (msuPAR2-Tg) corresponds to BC010309 in GenBank. Both msuPAR1 and msuPAR2 were under the control of AP2 promoter, followed immediately by a secretion signal peptide (Igκ). This experimental model system should result in the expression of suPAR protein in fat tissue, and release into the blood circulation thereafter. Genotyping positive founder mice were back-crossed with C57BL/6 mice for at least 5 generations to establish the colony. Both msuPAR1-Tg and msuPAR2-Tg mice are viable and fertile. Both lines of msuPAR-Tg mice presented similar body weight as compared to their non-Tg littermate controls. To enhance msuPAR production, regular rodent diet was replaced by HFD (Research Diets) when the mice were 2 months old, and the animals were kept on the high fat diet until there were sacrificed for further experiments. In order to generate double transgenic mice including msuPAR2-Tg/β3KO, msuPAR2-Tg/β3ΔRGT and msuPAR2-Tg/β3EGK mice, msuPAR2T-Tg mice crossed with with integrin β3 KO mice, integrin β3 cytoplasmic mutants β3ΔRGT and β3EGK mice respectively. To monitor proteinuria development and progression, spot urine was collected periodically from the above-mentioned mice. Urinary albumin and creatinine were determined using mouse albumin ELISA (Bethyl Labs, E99-134), and creatinine assay (Cayman Chemical, 500701) kits according to manufacturers' protocols.

Administration of Src inhibitors

Fifteen 10-12 weeks old msuPAR2-Tg mice were randomly divided into Src inhibitor treatment group (n=8) and vehicle control group (n=7). PP1 (Calbiochem) and Src inhibitor 1 (Sigma) were dissolved in DMSO and injected into msuPAR2-Tg mice via i.p at 5 mg/kg. Vehicle control mice received the same amount of DMSO. Spot urine was collected before and after treatment to monitor proteinuria in terms of albumin versus creatinine ratio.

Generation of rabbit anti-msuPAR2 antibody and Western blotting

Rabbit polyclonal anti-msuPAR2 antibody was developed against peptide CEQSASKRQLNPHTV via antibody services provided by Genscript. To detect msuPAR2 in blood circulation, 150 μl serum from each mouse was albumin-depleted with the aid of CaptureSelect multispecies albumin depletion product (ThermoFisher). The flow-through was then concentrated and equal amount of total protein from each sample was then loaded into SDS-PAGE gel for separation. Western blotting was performed following routine procedures and incubated with anti-msuPAR2 antibody (1:1000). To detect msuPAR2 in urine samples, 150 μl of urine obtained from each mouse was concentrated and washed with PBS, and the amount of total protein was quantitated. Equal amount of total urinary protein (120-150 μg) from each sample was processed for msuPAR2 detection as with serum samples. For peptide blocking, 5 times of msuPAR2 peptide was incubated with anti-msuPAR2 antibody for 30 min at RT,

and duplicated blots were processed with peptide-antibody mixture simultaneously as with msuPAR2 antibody for comparison.

Adipocyte tissue QPCR and immunohistochemistry

To examine msuPAR2 expression, gonadal fat tissues were excised out right after the mice were sacrificed. Total RNA was isolated with the RNeasy Lipid Tissue Mini Kit (Qiagen). QPCR was done with Bio-Rad's CFX96 Touch Real-Time PCR Detection System. The msuPAR2 primer pairs are as follows: forward, ACTACCGTGCTTCGGGAATG; reverse, AATGTTGGTCCCGTGACTGT.

For immunohistochemistry, paraffin embedded fat tissues were sectioned at 4 μm and rehydrated. The sections were heated at 95 degree with Antigen Unmasking solution (Vector Laboratories) for 5-10 min and treated with 3% hydrogen peroxide for 10 min, followed by 0.5% Triton-100 for one hour. After blocking with Avidin/Biotin Blocking Kit (ThermoFisher), the sections were incubated with rabbit anti-c-Myc antibody (1:400) overnight at 4 degree. Then the biotinylated goat-anti-rabbit IgG (Vector Laboratories) was added for 30 min. Thereafter, positive staining was revealed by ImmPACT DAB Peroxidase (HRP) Substrate (Vector Laboratories). Counterstain was performed with CAT Hematoxylin (Biocare Medical).

RNA Sequencing

Kidney glomeruli were isolated from msuPAR2-Tg mice and their littermate controls with the aid of dynabeads (ThermoFisher) as described elsewhere (28).

Total RNA of the glomeruli was isolated using RNeasy Mini Kit (Qiagen). RNA quality was assessed by Agilent Bioanalyzer 2100 and RIN scores of 7 or above were used. Libraries were prepared by the Illumina TruSeq RNA Preparation Kit. Samples were sequenced using Illumina HiSeq for single read 50 bp. The short reads were mapped to the UCSC mouse mm10 reference genome using Tophat (29,30). Next, the alignment results were processed using Cufflink to perform differential analysis both on gene and transcript level (31). The raw p-values were adjusted by Benjamini–Hochberg correction (32). The gene-set enrichment analysis was performed with DAVID (the Database for Annotation, Visualization and Integrated Discovery) (33).

Kidney Immunofluorescence

Frozen mouse kidney tissues were cut at 4 μm thickness and fixed with cold acetone for 10 min. After blocking with blocking solution (5% chicken normal serum for 1 h, samples were stained with goat anti-mouse uPAR antibody (1:200; R&D) for msuPAR1 and rabbit anti-mouse suPAR2 (1:200, in house) for msuPAR2. Rabbit anti-human podocin antibody (1:300, Sigma) or goat anti-human synaptopodin (1:300, Santa Cruz) was used to label podocytes respectively. The secondary antibodies for msuPAR1 labeling were Alexa Fluor 488-conjugated chicken anti-goat IgG (1:1000; Molecular Probes) and Alexa Fluor 594-conjugated chicken anti-rabbit IgG (1:1,000; Molecular Probes). For msuPAR2 labeling, the secondary antibody combination was Alexa Fluor 488-conjugated chicken anti-rabbit IgG (1:1000; Molecular Probes) and Alexa Fluor

594-conjugated chicken anti-goat IgG (1:1,000; Molecular Probes). Src phosphorylation was labeled with p-c-Src antibody (A96, 1:100, Santa Cruz). After sufficient washing, stained samples were mounted with ProLong Gold antifade reagent with DAPI (Molecular Probes, P36935). Images were obtained and analyzed using a LSM 700 confocal microscope (Carl Zeiss).

To explore the involvement of c-Src activity in human kidney diseases, a retrospective study with deidentified renal biopsy specimen was performed. The cryosections were fixed in 4% PFA for 15 min, followed by a brief heating process in a microwave oven. The staining procedures were described above with p-c-Src antibody (A96, 1:50, Santa Cruz), and synaptopodin antibody (P-19, 1:100, Santa Cruz).

Transmission electron microscopy

Transmission electron microscopy was performed as previously described (3). In brief, renal tissues were collected and dissected into 2x2 mm pieces. The tissues were fixed in 4% PFA O/N, washed 3 times in PBS and post fixed in 1% OsO_4. Tissues were washed in 0.1 M cacodylate buffer, dehydrated and embedded in Epon812 (EMS). 70 nm sections were mounted onto Formvar coated Ni slot grids (EMS). Grids were stained for 15 min in 5% uranyl acetate followed by 0.1% lead citrate for 5 min. Electron micrographs were obtained and analyzed using the Sigma HDVP Electron Microscope (Zeiss).

Detection of human uPAR isoforms in PBMC

To examine if human uPAR isoform exist, PBMCs were harvested from unidentified healthy blood donors and total RNA was isolated for qPCR. Primers or probes were designed to detect uPAR isoform 1 to 4 specifically. The respective amplicon sequences are as follows:

Isoform 1 fragment: 163 bp

CCCAATCCTGGAGCTTGAAAATCTGCCGCAGAATGGCCGCCAGTGTTACAG
CTGCAAGGGGAACAGCACCCATGGATGCTCCTCTGAAGAGACTTTCCTCAT
TGACTGCCGAGGCCCCATGAATCAATGTCTGGTAGCCACCGGCACTCACGA
ACCGAAAAAC.

Isoform 2 fragment: 96 bp

CTCACGAACGCTCACTCTGGGGAAGCTGGTTGCCATGTAAAAGTACTACTG
CCCTGAGACCACCATGCTGTGAGGAAGCCCAAGCTACTCATGTAT

Isoform 3 fragment: 88 bp

CACTGAGGTGAAGAAGTCCTGGAGCTTGAAAATCTGCCGCAGAATGGCCGC
CAGTGTTACAGCTGCAAGGGGAACAGCACCCATGGAT

Isoform 4 fragment: 75 bp

CTGAAATGCTGCAACACCACCAAATGCAACGAGGGCCCAAAACCGAAAAAC
CAAAGCTATATGGTAAGAGGCTGT

Statistical analyses

Statistical analysis was done with Prism 5.0 software (GraphPad). Difference between two groups was analyzed by Student's two-tailed *t*-test, or Mann-Whitney test when appropriate. Differences between more than two groups were

analyzed using one-way ANOVA. Differences between groups containing two variables were assessed by two-way ANOVA. In case not normally distributed data set, log transformation was performed. All data are presented as median and IQR, unless otherwise indicated. A P-value of ≤0.05 was considered significant.

Study approval

The animal study was approved by IACUC at Rush University Medical Center. All mice received humane treatment per protocol. The retrospective study with de-identified human biopsy specimen was approved by Rush institutional review boards (14051401).

Author Contributions

CW, JR developed the concept and designed the study. CW, JL, BA, KZ, JC, MM, BS, KHK, NJT, RRD, SH, SD, VP, SL, JM performed experiments. BDA and MAA carried out the structural studies. ZL, SJS provided β3 integrin knock-in mouse models. DJC, SL provided anonymous renal specimens. CW, JR, BA, JC, SS, SJS, JK analyzed and interpreted the cell, biochemical and animal data. CW and JR wrote the paper. SSH provided statistical input. BDA, JC, SS, SJS, JK, MAA and MT were involved in editing the paper.

Acknowledgements

This work was supported in part by National Institutes of Health (NIH) grants 1R01 DK101350. We are grateful for the contributions of the participants who made this study possible. In particular, we thank Dr. Hong Hu from Core for Research Informatics, University of Illinois at Chicago for assistance with RNA Seq analysis. We thank Dr. Yingcai Wang from University of Miami for assistance with suPAR transgenic mice. MAA was supported by RO1 DK48549, and RO1 DK088327. SJS was supported by HL78784.

References

1. Ploug M, Rønne E, Behrendt N, Jensen AL, Blasi F, Danø K. Cellular receptor for urokinase plasminogen activator. Carboxyl-terminal processing and membrane anchoring by glycosyl-phosphatidylinositol. *J Biol Chem*. 1991; 266(3):1926-33.
2. Thuno M, Macho B and Eugen-Olsen J. suPAR: The molecular crystal ball. *Dis Markers*. 2009; 27(3):157-172
3. Wei C, et al. Circulating urokinase receptor as cause for focal segmental glomerulosclerosis. *Nat Med*. 2011;17(8):952-60
4. Hahm E, et al. Bone marrow-derived immature myeloid cells are a main source of circulating suPAR contributing to proteinuric kidney disease. *Nat Med*. 2017; 23(1):100-106
5. Delville M, et al. A circulating antibody panel for pretransplant prediction of FSGS recurrence after kidney transplantation. Sci Transl Med. 2014 ;6(256):256ra136.
6. Hayek SS, et al. A tripartite complex of suPAR, APOL1 risk variants and αvβ3 integrin on podocytes mediates chronic kidney disease. *Nat Med*. 2017; 23(8):945-953
7. Hayek SS, et al. Soluble Urokinase Receptor and Chronic Kidney Disease. *N Engl J Med*. 2015 Nov 12;373(20):1916-25
8. Drechsler C, et al. Soluble Urokinase Plasminogen Activator Receptor and Outcomes in Patients with Diabetes on Hemodialysis. *Clin J Am Soc Nephrol*. 2017 Aug 7;12(8):1265-1273.

9. Schaefer F, Association of Serum Soluble Urokinase Receptor Levels With Progression of Kidney Disease in Children. *JAMA Pediatr*. 2017; 171(11):e172914. doi: 10.1001/jamapediatrics.2017.2914.
10. Luo S, Soluble Urokinase-Type Plasminogen Activator Receptor in Black Americans with CKD. *Clin J Am Soc Nephrol*. 2018;13(7):1013-1021.
11. Kristensen P, Eriksen J, Blasi F, Danø K. Two alternatively spliced mouse urokinase receptor mRNAs with different histological localization in the gastrointestinal tract. *J Cell Biol*. 1991;115(6):1763-71.
12. Pyke C et al. An alternatively spliced variant of mRNA for the human receptor for urokinase plasminogen activator. *FEBS Lett* 1993; 326:69-74
13. Spinale JM et al. A reassessment of soluble urokinase-type plasminogen activator receptor in glomerular disease. Kidney Int. 2015;87(3):564-74.
14. Cathelin D et al. Administration of recombinant soluble urokinase receptor per se is not sufficient to induce podocyte alterations and proteinuria in mice. *J Am Soc Nephrol*. 2014;25(8):1662-8
15. Lin L, Gårdsvoll H, Huai Q, Huang M, Ploug M. Structure-based engineering of species selectivity in the interaction between urokinase and its receptor: implication for preclinical cancer therapy. *J Biol Chem*. 2010;285(14):10982-92
16. Johnson RJ et al. Expression of smooth muscle cell phenotype by rat mesangial cells in immune complex nephritis. Alpha-smooth muscle actin is a marker of mesangial cell proliferation. *J Clin Invest.* 1991;87(3):847-58

17. Satchell SC, Anderson KL, Mathieson PW. Angiopoietin 1 and Vascular Endothelial Growth Factor Modulate Human Glomerular Endothelial Cell Barrier Properties. *J Am Soc Nephrol.* 2004;1 5(3):566-74.
18. Ablooglu AJ, Kang J, Petrich BG, Ginsberg MH, Shattil SJ. Antithrombotic effects of targeting alphaIIbbeta3 signaling in platelets. *Blood*. 2009;113(15):3585-92.
19. Liao Z et al. Interaction of kindlin-2 with integrin β3 promotes outside-in signaling responses by the αVβ3 vitronectin receptor. *Blood*. 2015;125(12):1995-2004.
20. Bain, J. et al. The selectivity of protein kinase inhibitors: a further update. *Biochem J* 2007; 408:297-315
21. Suh TT1, Nerlov C, Danø K, Degen JL. The murine urokinase-type plasminogen activator receptor gene*. J Biol Chem*. 1994;269(42):25992-8.
22. Wang J, Zhuang S. Src family kinases in chronic kidney disease. *Am J Physiol Renal Physiol*. 2017;313:F721-F728
23. Sweeney WE Jr, von Viger RO, Frost P, Avner ED. Src inhibition ameliorates polycystic kidney disease. *J Am Soc Nephrol.* 2008;19:1331-1341
24. Tesar V et al. Bosutinib versus placebo for autosomal dominant polycystic kidney disease. *J Am Soc Nephrol.* 2017;28:3404-3413
25. Mundel P et al. Rearrangements of the cytoskeleton and cell contacts induce process formation during differentiation of conditionally

immortalized mouse podocyte cell lines. *Exp Cell Res*. 1997;236(1):248-58.

26. Tang G, et al. EMAN2: an extensible image processing suite for electron microscopy. *J Struct Biol*. 2007;157(1):38-46.
27. Goddard TD, Huang CC, Ferrin TE. Software extensions to UCSF chimera for interactive visualization of large molecular assemblies. *Structure*. 2005 Mar;13(3):473-82.
28. Takemoto M et al. A new method for large scale isolation of kidney glomeruli from mice. *Am J Pathol*. 2002;161(3):799-805.
29. Trapnell C, Pachter L, Salzberg SL. TopHat: discovering splice junctions with RNA-Seq. *Bioinformatics*. 2009;25(9):1105-11.
30. Fujita PA et al. The UCSC Genome Browser database: update 2011. *Nucleic Acids Res*. 2011;39(Database issue):D876-82
31. Trapnell C et al. Transcript assembly and quantification by RNA-Seq reveals unannotated transcripts and isoform switching during cell differentiation. *Nat Biotechnol*. 2010;28(5):511-5.
32. Hochberg Y, Benjamini Y. More powerful procedures for multiple significance testing. *Stat Med*. 1990;9(7):811-8.
33. Dennis G Jr et al. Database for Annotation, Visualization, and Integrated Discovery. *Genome Biol*. 2003; 4(9): R60.

Figures

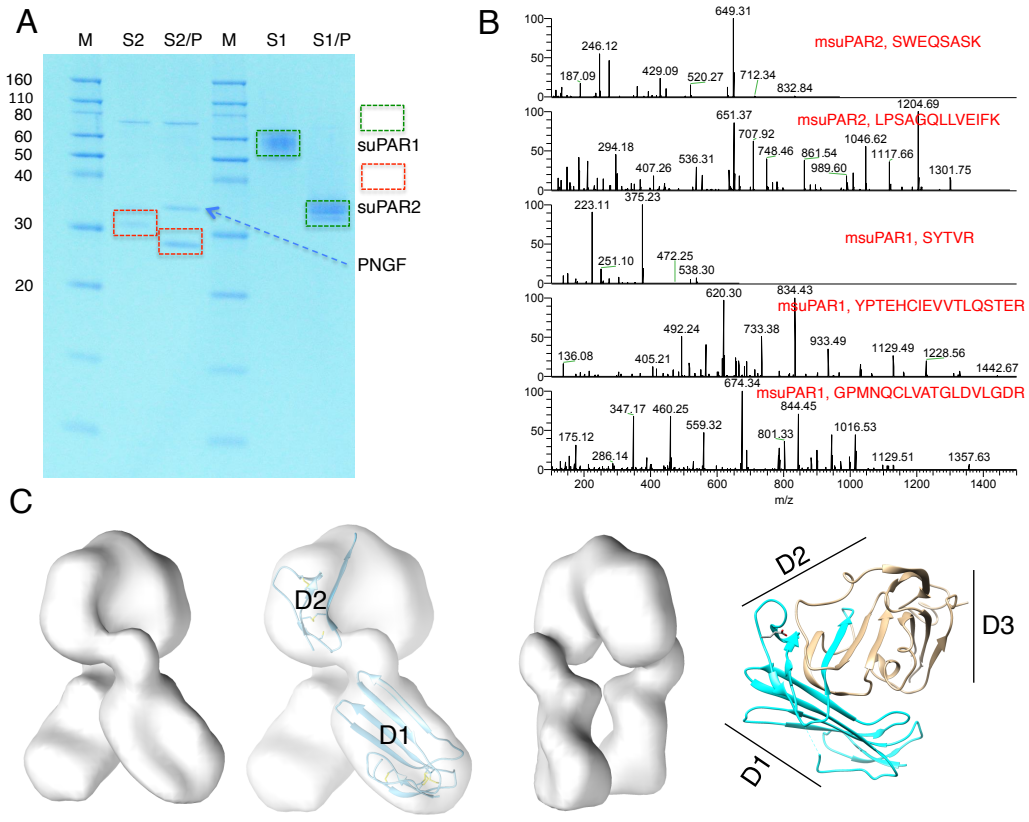

Figure 1. Characterization of msuPAR recombinant proteins. (**A**) SDS gel analysis of purified msuPAR1 and msuPAR2 before (S2 and S1) and after (S2/P and S1/P) de-glycosylation with PNGaseF. S1, msuPAR1; S2, msuPAR2; P, PNGaseF. (**B**) LC-MS verification of recombinant msuPAR1 and msuPAR2 proteins. Shown are representative mass spectra of identified peptides from the deglycosylated msuPAR proteins. (**C**) EM structure modeling of msuPAR2. The isosurface has been set to enclose 100% of the expected protein mass. The second to the left is the same map as the first but displays the fit of domains D1 and the expressed portion of domain D2 in the map. The additional sequences following the splice junction have not been modeled. The third is the same map

as the first but rotated 90°. The fourth shows the ribbon diagram of the msuPAR1 structure (pdb id 3LAQ) for comparison. The region included in msuPAR2 is indicated in blue. Locations of the 3 domains of msuPAR1 are indicated with black lines.

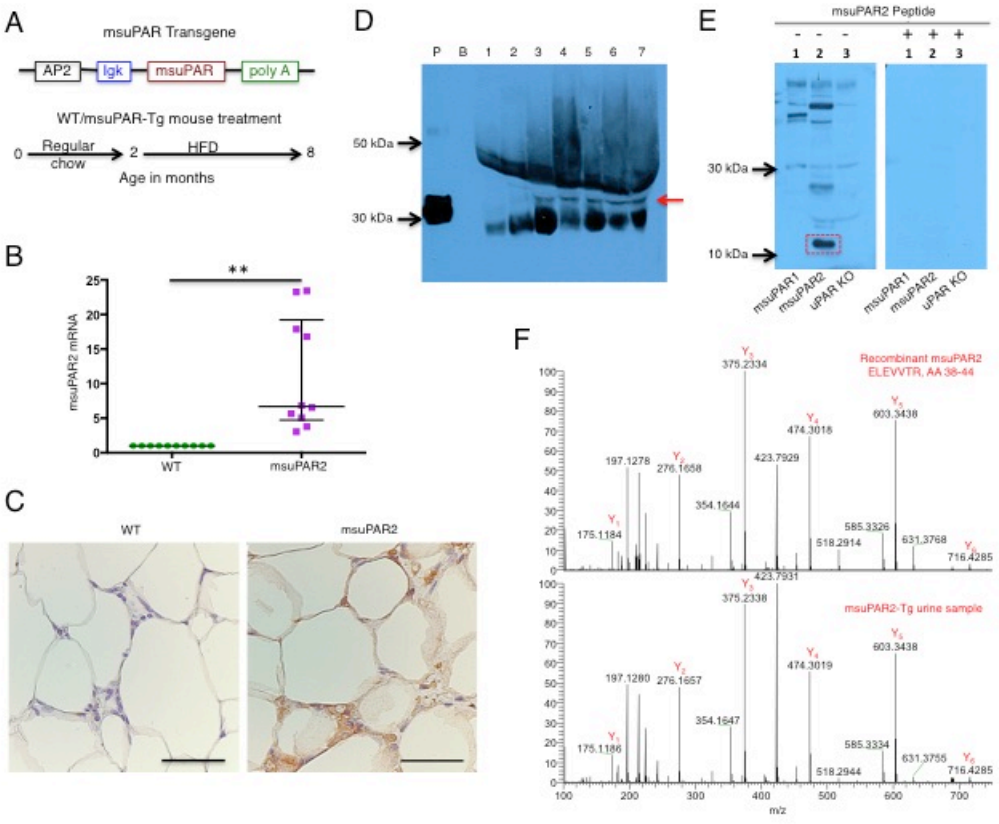

Figure 2. Detection of msuPAR2 in adipocytes, serum and urine. (**A**) Illustrations of msuPAR2 transgene (Tg) construction and msuPAR2-Tg mouse treatment. (**B**) Quantitative PCR analysis of muPAR2 in fat tissues. The value was calculated as a ratio of muPAR2 differential expression between littermate controls (WT) and msuPAR2-Tg mice over that of housing keeping gene GADPH. muPAR2 mRNA was increased significantly as compared to littermate controls. Mann-Whitney test, ** $p<0.01$. (**C**) Localization of msuPAR2 in adipocytes. As msuPAR2 carries c-Myc tag, immunohistochemistry was performed with a rabbit anti-Myc antibody. msuPAR2 could be appreciated in adipocytes of msuPAR2-Tg mice, but not in littermate control mice. Scale bar, 50

μm. (**D**) Detecting msuPAR2 in circulating blood in msuPAR2-Tg mice. Albumin depleted sera were separated by NuPAGE gel and processed for western blotting with rabbit anti-msuPAR2 antibody. P, recombinant msuPAR2 protein; B, blank without protein samples; Lane 1 represents uPAR KO sera; Lane 2, msuPAR1-Tg sera; Lane 3 to Lane 7, sera from different msuPAR2-Tg mice. Images shown are representatives of three different experiments. Red arrow indicates msuPAR2. (**E**) Detecting msuPAR2 in urine. Processed urine samples were separated by SDS-PAGE and blotted with a customized rabbit anti-msuPAR2 antibody. A band at 10-15 kDa (highlighted in red rectangle) was identified in msuPAR2-Tg but not in msuPAR1-Tg nor in uPAR KO mice. Pre-incubation the antibody with msuPAR2 peptide nullified the band. (**F**). Verification of msuPAR2 fragment by LC-MS analysis. The msuPAR2 fragment identified by western blot was processed for MS analysis. Multiple peptides in N-terminal region were detected. Shown is one of these peptides (bottom panel), which matches very well with the spectrum of the peptide from recombinant msuPAR2 protein (top panel).

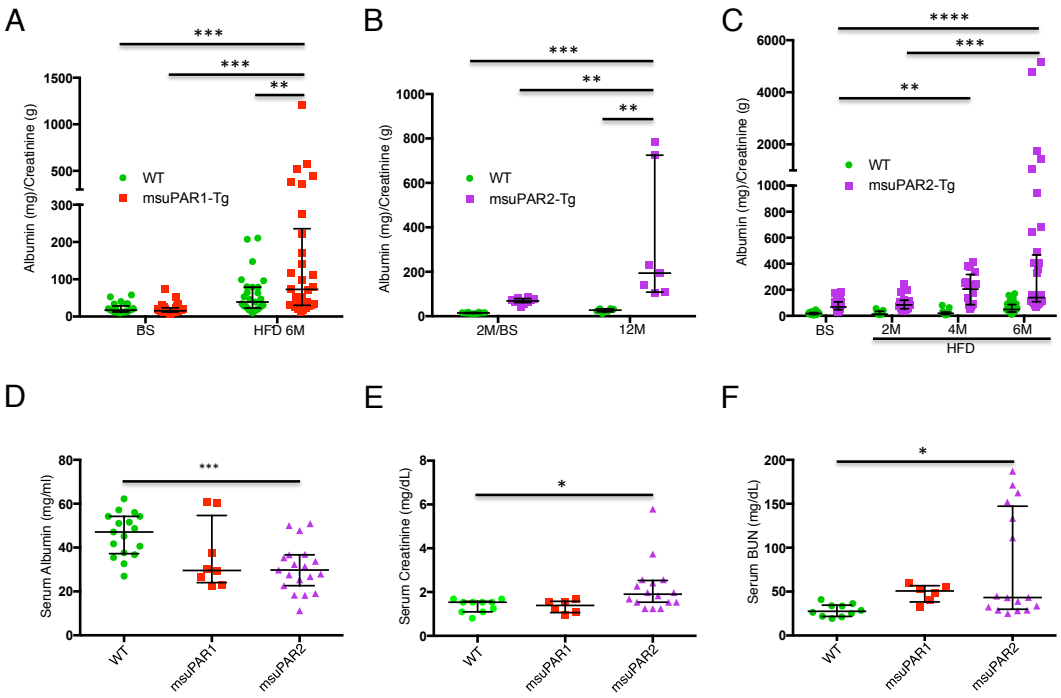

Figure 3. msuPAR2-Tg mice develop progressive proteinuria and severe kidney dysfunction. (**A**) Proteinuria profiling in msuPAR1-Tg mice. Proteinuria, in terms of albumin/creatinine ratio, which was absent before HFD treatment at baseline, developed in msuPAR1-Tg mice after 6 months into HFD. n=25 for WT/BS, n=26 for msuPAR1-Tg/BS, n=27 for WT/HFD6M, n=30 for msuPAR1-Tg/HFD6M. Two-way ANOVA, data were log-transformed to normal distribution. (**B**) Spontaneous proteinuria in msuPAR2-Tg mice. Without HFD treatment, proteinuria was evident in msuPAR2-Tg mice at 2 months old and increased significantly by 12 months old. n=9 for 2M/BS, n=7 for 12M. Two-way ANOVA. (**C**) With HFD treatment, msuPAR2-Tg mice developed accelerated and progressive proteinuria over a period of 6 months. n=30 for WT/BS, n=26 for msuPAR2-Tg/BS, n=9 for WT/HFD2M, n=16 for msuPAR2-Tg/HFD2M, n=13 for

WT/HFD4M, n=16 for msuPAR2-Tg/HFD4M, n=31 for WT/HFD6M, n=36 for msuPAR-Tg/HFD6M. WT, littermate control mice. BS, baseline (at 2 months old, before HFD treatment). HFD, high fat diet. Two-way ANOVA. Data were log-transformed to normal distribution. (**D**) Serum albumin decreased significantly in HFD treated msuPAR2-Tg mice as compared to WT (littermate control) mice. n=17 for WT, n=8 for msuPAR1-Tg, n=19 for msuPAR2-Tg mice. One-way ANOVA. (**E**) Serum creatinine increased significantly in HFD treated msuPAR2-Tg mice. n=10 for WT, n=6 for msuPAR1-Tg, n=16 for msuPAR2-Tg mice. One-way ANOVA. (**F**) Serum BUN levels increased significantly in HFD treated msuPAR2-Tg mice. n=10 for WT, n=6 for msuPAR1-Tg, n=16 for msuPAR2-Tg mice. One-way ANOVA. For all data sets, * $p<0.05$, ** $p<0.01$, *** $p<0.001$, **** $p<0.0001$.

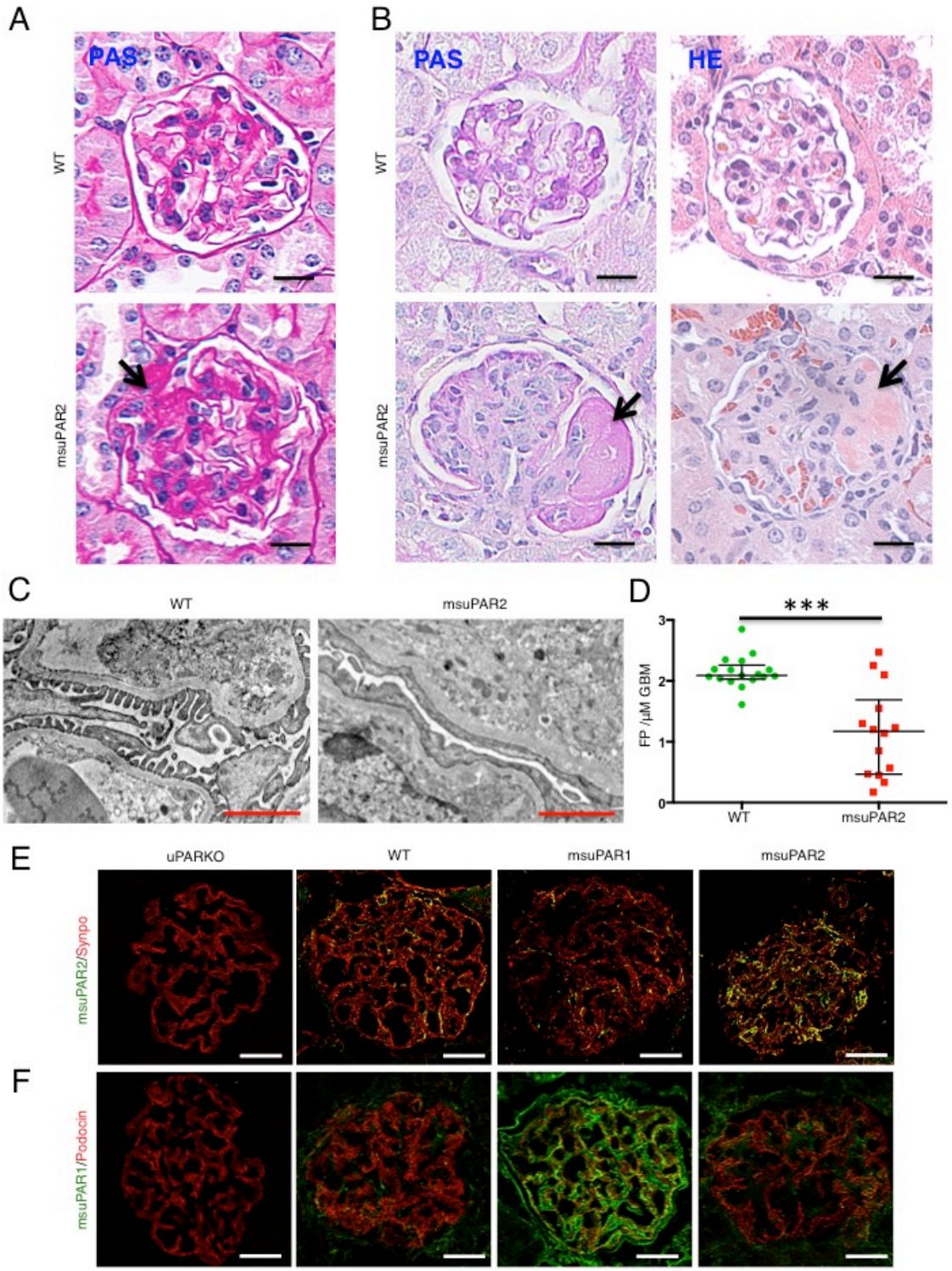
A
PAS
WT
msuPAR2
B
PAS
HE
WT
msuPAR2
C
WT
msuPAR2
D
***
FP /µM GBM
3
2
1
0
WT
msuPAR2
E
uPARKO
WT
msuPAR1
msuPAR2
msuPAR2/Synpo
F
msuPAR1/Podocin

Figure 4. msuPAR2-Tg mice present FSGS-like kidney pathology. (**A**). PAS staining of kidney sections from spontaneous non-HFD treated mice. Segmental glomerular sclerosis was appreciated in some glomeruli of msuPAR2-Tg mice. In contrast, no abnormality was observed in littermate control, WT mice. Scale bar, 20 μm. Arrow shows sclerotic area. (**B**). Kidney histology of HFD treated mice. Left panel, PAS staining; Right panel, H&E staining. Histological features of advanced FSGS were observed in HFD-treated msuPAR2-Tg mouse kidneys. Scale bar, 20 μm. Arrow shows sclerotic area. Transmission electron microscope (TEM) examination (**C**) and analysis (**D**) indicate that foot process (FP) effacement significantly increased with msuPAR2-Tg mice. Data was represented by the FP counts per μm of glomerular basement membrane (GBM). n=17 for WT; n=14 for msuPAR2-Tg. *** $p<0.001$. Student T-test. Scale bar, 1 μm. (**E**) Localization of msuPAR2 in the glomeruli. Kidney cryosections were performed with double immunofluorescent stainings with anti-msuPAR2 antibody and anti-synaptopodin antibody. Syno, synaptopodin was used as a podocyte marker. Co-localization of msuPAR2 (green) with synapopodin (red) was appreciated as brownish color. (**F**) Localization of msuPAR1 in the glomeruli by msuPAR1 antibody. As compared to WT and msuPAR2-Tg mice, the abundance of msuPAR1 was clearly observed in the msuPAR1-Tg mice. Scale bar, 20 μm. WT, littermate control mice; uPAR KO, *Plaur*$^{-/-}$ mice. Negative staining of both msuPAR1 and msuPAR2 in uPAR KO mice indicates the specificities of the suPAR antibodies employed.

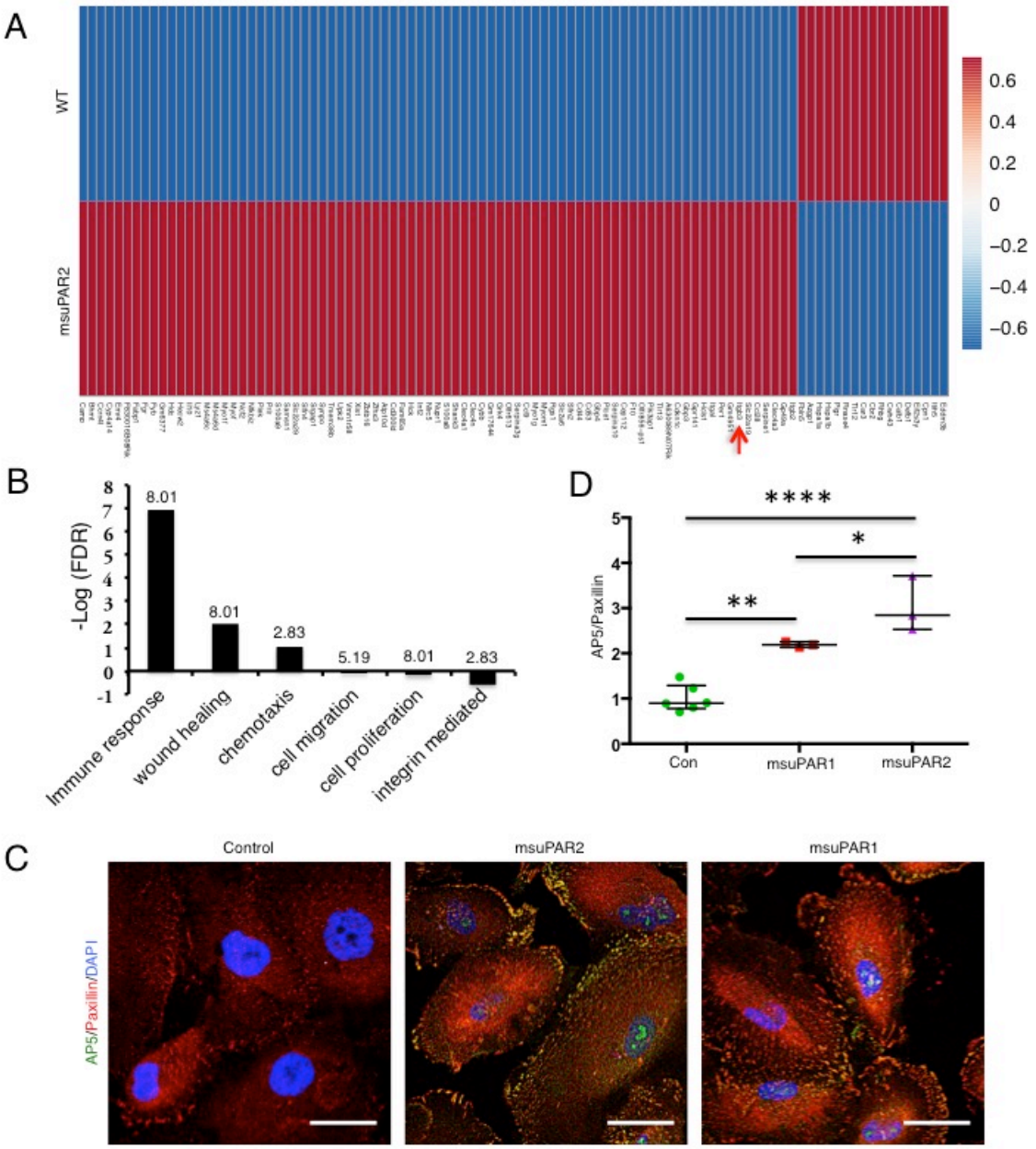

Figure 5. Glomerular β3 integrin expression is increased in msuPAR2-Tg mice. (**A**) RNA sequencing of msuPAR2-Tg mouse glomeruli. Differentially expressed genes are shown in the heatmap. Red, high transcript levels; Blue, low transcript levels. n=7 for suPAR2-Tg mice; n=3 for littermate controls. Red arrow indicates *Itgb3*. (**B**) Differentially expressed pathways identified by gene-

set enrichment analysis via DAVID (the Database for Annotation, Visualization and Integrated Discovery). Number above the bar represents counts in percentage. FDR, false discovery rate. (**C**) and (**D**) msuPAR2 induces β3 integrin activity on human podocytes. Cultured human podocytes were treated with purified msuPAR2 or msuPAR1 protein at 1 ng/ml and examined for β3 integrin activation as indicated by AP5 staining intensity. Activated β3 integrin co-localized with paxillin. Control received same amount of BSA. Scale bar, 50 μm *p<0.05, **p<0.01, *** p<0.0001.

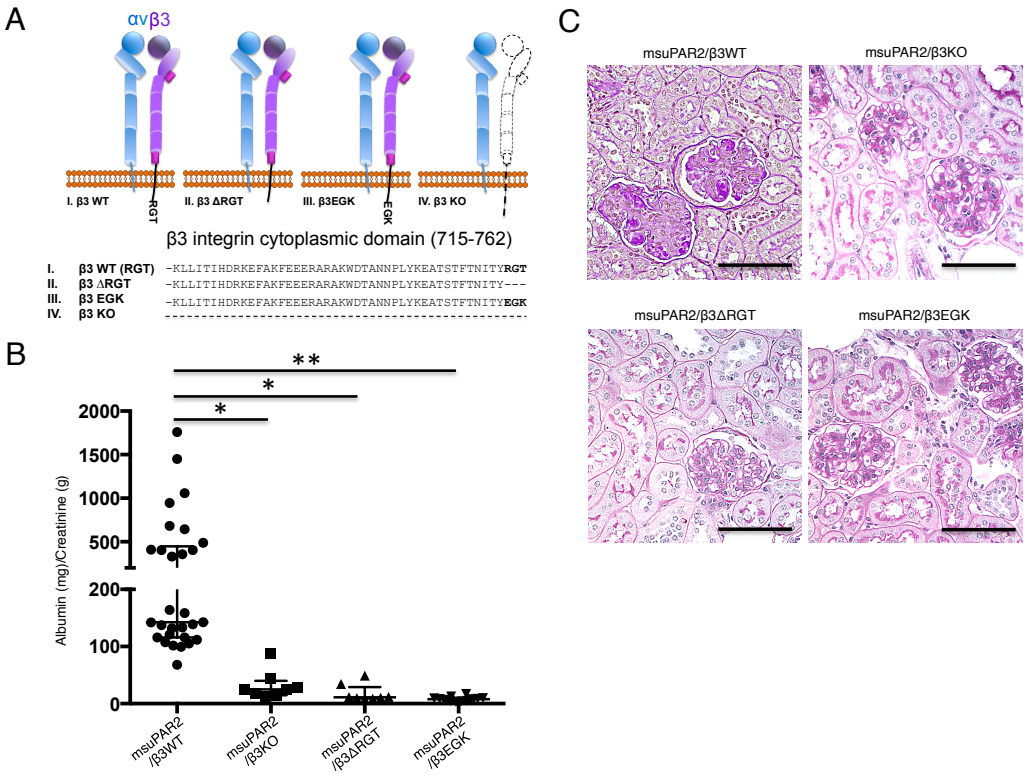

Figure 6. msuPAR2 induced kidney disease requires the presence of intact β3 integrin. (**A**) Schematic delineations of the cytoplasmic domain of three genetically engineered β3 integrin mouse models. Dashed line represents absence. In terms of β3 integrin KO, αv integrin could dimerize with β5 or other integrin beta subunit. (**B**) Proteinuria assay. Proteinuria is shown as albumin (mg)/creatinine (g) ratio obtained from spot urine samples. n=29 for msuPAR2-Tg, n=8 for msuPAR2-Tg/β3KO, n=8 msuPAR2-Tg/β3ΔRGT, n=12 for msuPAR2-Tg/β3EGK mice. * $p<0.05$, ** $p<0.01$, One-way ANOVA test. (**C**) Kidney histology. 5 to 6 months after HFD treatment, all mice were sacrificed for kidney histological analysis with PAS staining. Shown are representative kidney sections from msuPAR2/β3WT, msuPAR2/β3KO, msuPAR2/β3ΔRGT and msuPAR2/β3EGK respectively. Scale bar, 100 μm. Except in msuPAR2/β3WT,

FSGS-like glomerulopathy was not appreciated in msuPAR2/β3KO, msuPAR2/β3ΔRGT or msuPAR2/β3EGK mice.

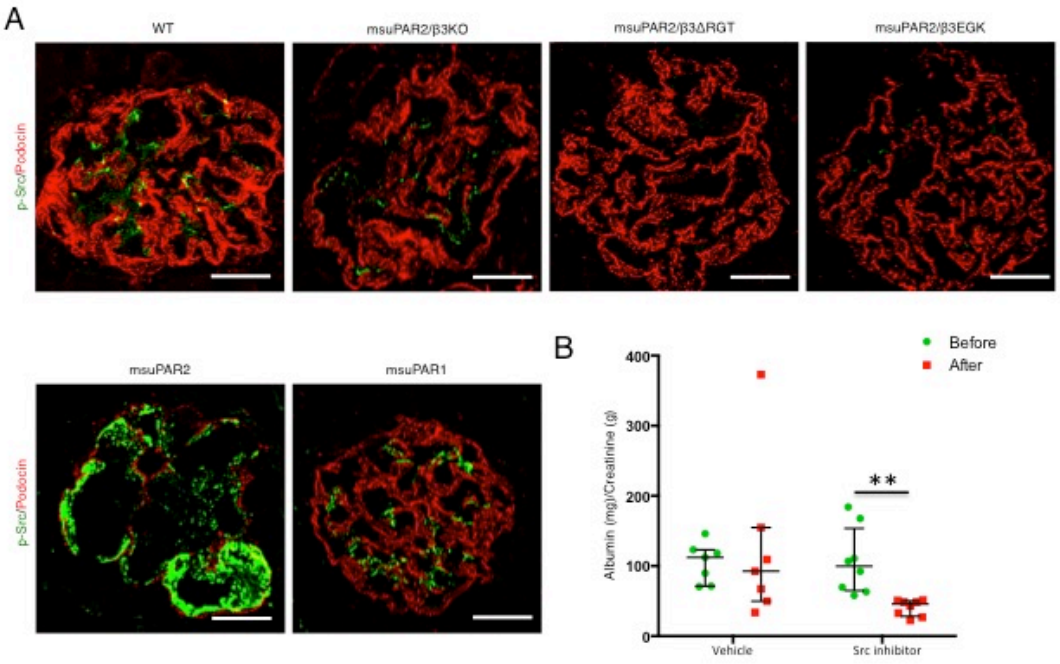

Figure 7. Blocking Src activity reduces proteinuria in msuPAR2-Tg mice. (**A**) Glomerular Src activity was examined by immunofluorescent staining the kidney cryosections with p-Src monoclonal antibody (green color). Podocin was used as a podocyte marker (red color). Shown are the representative glomeruli with p-Src immunofluorescent staining. As indicated by the p-Src staining intensity, glomerular Src phosphorylation was readily observed in the kidney sections from msuPAR2-Tg, but not from other investigated mice. Scale bar, 20 μm. (**B**) Treatment with Src inhibitors lowered proteinuria in msuPAR2-Tg mice. Both PP1 and Src inhibitor 1 (5 mg/kg) were administered into the randomly grouped msuPAR2-Tg mice intraperitoneally, with vehicle controls received same amount of DMSO. n=8 for Src inhibitor group, n=7 for vehicle control group. 72 hours after treatment, proteinuria was significantly reduced by Src inhibitor

treatment. Two-way ANOVA, data were log-transformed to normal distribution, ** $p<0.01$.

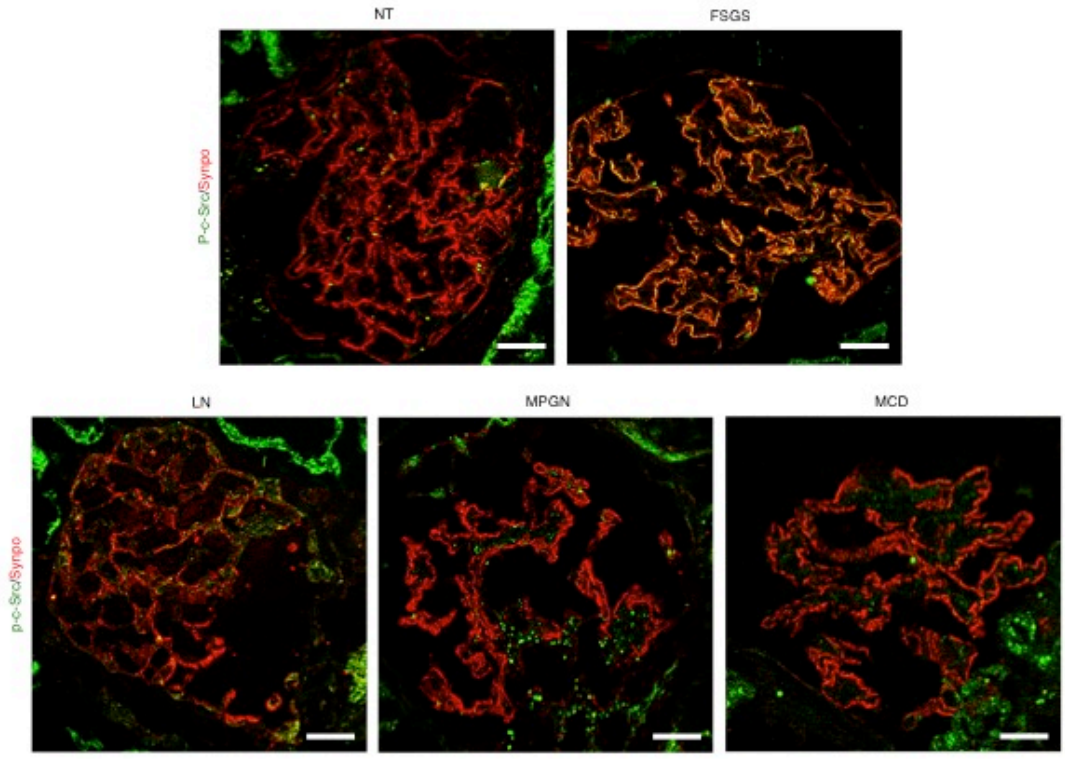

Figure 8. Glomerular c-Src activity is increased in human FSGS kidney. Immunofluorescent staining with p-c-Src antibody was performed for the frozen sections of deidentified human kidney biopsies. Synpo (synaptopodin) was used as a podocyte marker. Shown are representative of 4 batches of immunostaining. While minimal amount of c-Src phosphorylation was observed in the glomeruli of healthy donors (n=3), glomerular p-c-Src intensity was increased in 6 out of 10 FSGS patients. Overlap of p-c-Src (green color) and synpo (red color), indicating that p-c-Src was localized in podocytes. Of note, only 11 out of 24 observed glomeruli were positive for p-c-Src, from which 64% were focal, 36% were globally but not evenly. In contrast, the increase of pSrc was not observed in other glomerular disease including SLE (n=2), MPGN (n=2) and MCD (n=4). Scale bar, 20 μm. NT, normal kidney tissue; FSGS, focal segmental

glomerusclerosis; LN, lupus nephritis; MPGN, mesangioproliferative glomerulosclerosis; MCD, minimal change disease.